

Supporting Information for

Carrier-gas Assisted Vapor Deposition for Highly Tunable Morphology of Halide Perovskite Thin Films

Catherine P. Clark,^a Bryan Voigt,^a Eray S. Aydil^b and Russell J. Holmes^a

^a Department of Chemical Engineering and Materials Science University of Minnesota, Minneapolis MN 55455

^b Department of Chemical and Biomolecular Engineering, Tandon School of Engineering, New York University, Brooklyn, NY, 11201

Experimental Methods

Substrate Preparation

Quartz, silicon, and ITO-coated glass (15 Ω /sq, Nin Yan Technology Limited) substrates were cleaned *via* sequential sonication in baths of diluted tergitol, deionized water, and acetone. Substrates were then boiled in isopropanol, dried with N_2 , and treated with UV-ozone for 15 minutes. For PEDOT:PSS films on ITO, PEDOT:PSS solution (CLEVIOS™ P VP Al 4083, Heraeus) was filtered with a 0.45 μ m filter, and then spin-coated at 4000 rpm for 40 seconds. Films were baked in N_2 at 150 $^\circ$ C for 30 minutes. For compact TiO_2 films on ITO, a TiO_2 solution was prepared by the addition of 0.7 mL titanium isopropoxide (Sigma Aldrich, 97%) to 10 mL isopropanol and 10 μ L HCL. After filtering with a 0.2 μ m filter, this solution was spin-coated at 3000 RPM for 45 seconds. Films were then sintered in air for 30 minutes at 475 $^\circ$ C.

Perovskite Film Deposition *via* CGAVD

Prior to each deposition, the inside of the deposition chamber and source ampoules were wiped with acetone and isopropanol, and then baked at temperatures > 300 $^\circ$ C and pressures < 20 mTorr for at least 1 hour. Cleaned substrates were attached to a copper plate with 1 – 4 layers of thermally conductive silicone pads (Wathai 0.5 mm thick, 2.0 W/mK). This plate was then screwed tightly onto the substrate holder so as to provide intimate thermal contact. Source materials were used as received: $SnBr_2$ (BTC, 99% purity), MABr (Sigma Aldrich, 98% purity), MAI (Lumtec, 99.5% purity), SnI_2 (Alfa Aesar, 99.999% purity). For deposition, ~ 100 mg of source material was packed tightly into the fritted-end of an extra coarse gas dispersion tube (170 to 220 μ m pore size) inside of a N_2 glovebox. Source material frits were then inserted into the deposition chamber using a linear feedthrough. Source material frits are discarded once $\sim 50\%$ of the source material is consumed. When not being used, source materials were stored in a N_2 glovebox. With the source materials and substrates loaded, the chamber was evacuated and held at a pressure of < 20 mTorr for 5 minutes. The substrate cooling water circulator is turned on, and the desired substrate temperature is achieved through use of a flow control valve and/or the recirculating water temperature. The chamber was then allowed to equilibrate at the deposition temperature T_g , pressure (P), dilution gas flow rates (\dot{V}_{CG}), and substrate temperature (T_s) for 1 hour. This time required for thermal equilibration (~ 1 hour) was determined by time-dependent temperature measurements using the thermocouples imbedded in the source material linear actuators. During this time, the source materials remain cold and the carrier gas is turned off. This is critical as our system does not contain source or substrate shutters and so relies on T_i and $\dot{V}_{CG,i}$ to start and stop deposition. Once the chamber temperatures, flow rates, and pressures have reached steady-state equilibrium, the source materials are positioned at distances corresponding to the desired temperature. The source temperature(s) are monitored and their axial position adjusted until the desired temperature is reached and remains stable (typically takes ~ 10 minutes). At this time, the N_2 carrier gases ($\dot{V}_{CG,i}$) for each source material are turned to the desired rate using a mass flow controller – this is considered “time zero” for deposition, as source material vapor is now being convectively transported down the chamber. The deposition is ended by quickly (< 5 seconds) pulling the source materials back into the cold-portion of the N_2 manifold and simultaneously turning off $\dot{V}_{CG,i}$. Films are stored in the dark in a nitrogen glovebox except for when they are actively being characterized.

Film Characterization

Film thicknesses were measured either using a J.A. Wollam Spectroscopic Ellipsometer and Cauchy model fit, or estimated from absorbance measured using a CARY 7000 UV-VIS-IR spectrometer. Photoluminescence spectra were measured using a Photon Technology International QuantaMaster 4 Fluorometer under N₂ purge. X-ray diffraction was collected using either a Bruker D8 Discover 2D diffractometer (Co K α radiation, $\lambda=1.7889$ Å) or a PANalytical X'pert PRO diffractometer (Co K α radiation, $\lambda=1.7889$ Å). Scanning Electron Microscope (SEM) images were obtained using a JEOL 6500 instrument with 5 kV potential and ~ 30 mA current.

Resistivity and Hall Effect Measurements

MASnX₃ (X=I,Br) films were deposited *via* CGAVD onto Ag (vacuum thermal evaporation, VTE), Au (VTE) or ITO contacts in a van der Pauw geometry. Four terminal resistance and Hall effect measurements were measured DC with a Keithley 2400 or a combination of a Keithley 220 current source and a Keithley 2002 voltmeter at 280 K in a Quantum Design Physical Property Measurement System (PPMS) equipped with a 9 T superconducting magnet. Checks were made for ohmicity, contact resistance, and Joule heating.

Material Flux and Deposition Rate Derivation for CGAVD System

The following derivation is based on the work of Shtein et al.,¹ and addresses material deposition rate in a carrier-gas assisted vapor deposition (CGAVD) system operating at steady-state and in continuum flow (i.e. Knudsen # < 0.01).

Table S1 Variables used in deposition rate derivation along with typical values for the experiments reported herein.

Variable	Description	Typical Values	Unit
Six independently controlled experimental parameters			
T_i	source material temperature for species i	375 – 500	K
T_g	temperature of gas in chamber as it reaches the substrate	500 – 600	K
$r_{dep,i}$	deposition rate of species i in Å/s	0.01 – 10	Å/s
$\dot{V}_{CG,i}$	carrier gas flow rate for species i measured @ mass flow controller (MFC) (i.e. ambient pressure measurement)	3E-8 – 2E-7	m ³ /s
\dot{V}_{DIL}	dilution gas flow rate measured @ mass flow controller (MFC) (i.e. ambient pressure measurement)	0 – 4E-6	m ³ /s
P	deposition pressure	40 – 1400	Pa
Fit Parameters			
ΔH_i^\ddagger	sublimation enthalpy of source material i	8E4 – 2E5	J / mol
$C_{1,i}$	material specific constant that arises from integrating the Clausius-Clapeyron equation to calculate source material equilibrium vapor pressure	10 – 1000	Pa
$C_{2,i}$	constant that arises from integrating the Clausius clapeyron equation to calculate source material equilibrium vapor pressure	400 – 700	K
$C_{3,i}$	constant relating boundary layer thickness and Reynolds number.	~ 0	m
Known and or Fixed Parameters			
R	universal gas constant	8.314	J / molK
A_{SH}	Area of substrate holder	0.0032	m ²
A_{chamb}	Cross-sectional area of chamber	0.0046	m ²
M_i	Molar mass of source material	variable	kg/mol
M_{N_2}	Molar mass of nitrogen gas	28,014	kg/mol

ρ_i	Source material density	variable	$\frac{\text{kg}}{\text{m}^3}$
P_0	Standard pressure	101325	Pa
T_0	Standard temperature	293.15	K
γ	Empirical constant from Chapman-Enskog theory	50.7	$\frac{\text{Pa m}^2}{\text{K}^{3/2} \text{s}}$
σ_i^2	average collision diameter	~ 5	Å
Ω_i	Temperature dependent collision integral	~ 1	unitless
Calculated and/or Intermediate Quantities			
$r_{\text{dep},i}$	deposition rate in A/s	0.05 – 5	A/s
$r_{\text{conv},i}$	deposition rate	$\sim r_{\text{dep}}$	mol/s
$r_{\text{diff},i}$	deposition rate	$\rightarrow \infty$	mol/s
r_i	flux rate of species i in mol/s at the surface of the substrate	1E-6 - 1E-8	mol/s
D_i	diffusivity of vapor in carrier gas	1E-4	$\frac{\text{m}^2}{\text{s}}$
δ	Velocity boundary layer thickness (of normal, columnated flow impinging on substrate)	$\rightarrow \infty$	m
$\text{Conc}_{\text{BL},i}$	Concentration of sublimed source material vapor in carrier gas at boundary layer interface	variable	mol /m ³
$\dot{V}_{\text{CG},i,\text{chamb}}$	Carrier gas flow at deposition pressure	1E-4 – 2E-3	m ³ /s
$\dot{V}_{\text{DIL},\text{chamb}}$	Dilution gas flow rate at deposition pressure	0 – 3E-2	m ³ /s
$\dot{V}_{\text{total},\text{chamb}}$	Total gas flow rate ($\sum \dot{V}_{\text{CG},i,\text{chamb}} + \dot{V}_{\text{DIL},\text{chamb}}$) at deposition pressure	1E-4 – 4E-2	m ³ /s
\dot{V}_{total}	Total gas flow rate ($\sum \dot{V}_{\text{CG},i} + \dot{V}_{\text{DIL}}$) at ambient pressure	3E-8 – 5E-6	m ³ /s
$P_{i,\text{eq}}$	Source material equilibrium pressure @ source material temperature	variable depending on source material	Pa
P_{BL}	Source material partial pressure @ velocity boundary layer, relevant for the diffusion across the velocity boundary layer driven by the source material concentration gradient	$P < P_{\text{BL}} < P + \frac{1}{2} \rho * v^2$	Pa
T_{BL}	Gas temperature at/of the boundary layer relevant for diffusion across the boundary layer	$T_s < T_{\text{BL}} < T_g$	K
Re	Reynolds #	0.1 – 10	dimensionless
v	Flow velocity	0.01 - 0.5	m/s

Single Material Deposition Rate Derivation

The deposition rate of material i ($r_{\text{dep},i}$) on the substrate will depend both on the flux of material that reaches the surface of the substrate (r_i) and the rate that molecules stick and unstick to the substrate (often referred to as the “sticking coefficient”). The sticking coefficient is quite challenging to parametrize analytically, as it depends on T_s and the surface properties of the film, including any reactions with other species. To capture the most general case, we can write

$$r_{\text{dep},i} = r_i \cdot f(T_{\text{sub}}, \text{film surface properties, rxns}). \quad \text{eqn S1}$$

The rate that source material molecules reach the surface of the substrate (r_i) depends on the rate at which the source material is convectively transported from the source ($r_{\text{conv},i}$) and the rate at which the source material diffuses through the boundary layer of thickness δ at the surface of the substrate ($r_{\text{diff},i}$). See Fig. S1a for a depiction of these transport regions. We can thus write

$$\frac{1}{r_i} = \frac{1}{r_{\text{conv},i}} + \frac{1}{r_{\text{diff},i}}, \quad \text{eqn S2}$$

or, rearranging,

$$r_i \left(\frac{\text{mol}}{\text{s}} \right) = \frac{r_{\text{conv},i}}{1 + \frac{r_{\text{conv},i}}{r_{\text{diff},i}}}, \quad \text{eqn S3}$$

Assuming steady state operation and conservation of mass in the chamber, $r_{\text{conv},i}$ is equal to the rate of source material flux out of the source material ampoule. Assuming ideal gas behavior, this quantity depends on the source material vapor pressure in the ampoule (P_i), the source material temperature (T_i), and the carrier-gas flow rate inside the chamber ($\dot{V}_{\text{CG},i,\text{chamb}}$):

$$r_{\text{conv},i} = \dot{V}_{\text{CG},i,\text{chamb}} \cdot \frac{P_i}{RT_i} \quad \text{eqn S4}$$

Note that $\dot{V}_{\text{CG},i,\text{chamb}}$ is related to the volumetric carrier gas flowrate controlled by the mass flow controllers (i.e. the flow rate measured outside of the chamber @ ambient temperature and pressure):

$$\dot{V}_{\text{CG},i,\text{chamb}} = \dot{V}_{\text{CG},i} \cdot \frac{P_0}{P} \cdot \frac{T_g}{T_0}. \quad \text{eqn S5}$$

Within the source material ampoule *at steady state*, the convective rate of transport of material out of the ampoule ($r_{\text{conv},i}$) must be in balance with the relative rates of source material evaporation ($r_{\text{evap},i}$) and condensation ($r_{\text{cond},i}$):

$$r_{\text{conv},i} = r_{\text{evap},i} - r_{\text{cond},i} \quad \text{eqn S6}$$

where $r_{\text{evap},i}$ depends on the equilibrium vapor pressure ($P_{i,\text{eq}}$), and a kinetic factor of evaporation ($k_{\text{evap},i}$):

$$r_{\text{evap},i} = k_{\text{evap},i} \cdot P_{i,\text{eq}} \quad \text{eqn S7}$$

and $r_{\text{cond},i}$ depends on the *actual* vapor pressure in the ampoule (P_i), and a kinetic factor of condensation ($k_{\text{cond},i}$):

$$r_{\text{cond},i} = k_{\text{cond},i} \cdot P_i \quad \text{eqn S8}$$

Combining equations S4 and S6-S8, we get

$$P_i = P_{i,\text{eq}} \cdot \frac{k_{\text{evap},i}}{\dot{V}_{\text{CG},i,\text{chamb}}/RT_i + k_{\text{cond},i}}. \quad \text{eqn S9}$$

Using Clausius-Clapeyron:

$$P_{i,\text{eq}} = C_{1,i} e^{\frac{-\Delta H_i^{\text{S}}}{R} \left(\frac{1}{T_i} - \frac{1}{C_{2,i}} \right)}, \quad \text{eqn S10}$$

where $C_{1,i}$, $C_{2,i}$, and ΔH_i^{S} are material-specific constants.

Combining eqns S4, S5, S9, and S10, we arrive at:

$$\begin{aligned} r_{\text{conv},i} &= \frac{P_0}{RT_0} \cdot \frac{\dot{V}_{\text{CG},i}}{T_i} \cdot \frac{T_{\text{gas}}}{P} \cdot P_i, & \text{eqn S11} \\ P_i &= C_{1,i} e^{\frac{-\Delta H_i^{\text{S}}}{R} \left(\frac{1}{T_i} - \frac{1}{C_{2,i}} \right)} \cdot \frac{k_{\text{evap},i}}{\dot{V}_{\text{CG},i, \text{chamb}}/RT_i + k_{\text{cond},i}}. \end{aligned}$$

The flux of material i across the boundary layer of thickness δ will be driven by the concentration gradient across the boundary layer ($\Delta C_i/\delta$) according to 1D Fick's law at steady state:

$$\text{Flux}_i = -D_i \cdot \frac{\Delta C_i}{\delta}. \quad \text{eqn S12}$$

If we assume a sticking coefficient of ~ 1 (reasonable for cold substrate temperatures), we implicitly assume that the concentration of source material vapor at the substrate surface is zero, so $\Delta C_i \rightarrow \text{Conc}_{\text{BL},i}$. Thus the rate of diffusion of species i across the substrate holder can be written as

$$r_{\text{diff},i} \left(\frac{\text{mol}}{\text{s}} \right) = \text{Flux}_i \cdot A_{\text{SH}} = D_i \cdot \frac{\text{Conc}_{\text{BL},i}}{\delta} \cdot A_{\text{SH}}. \quad \text{eqn S13}$$

The source material concentration at the boundary layer ($\text{Conc}_{\text{BL},i}$), is equal to the concentration of source material concentration leaving the ampoule ($\frac{P_i}{RT_i}$), multiplied by the flow dilution ratio (ratio of carrier-gas to total N_2 flow):

$$\text{Conc}_{\text{BL},i} = \frac{P_i}{RT_i} \cdot \frac{\dot{V}_{\text{CG},i}}{\dot{V}_{\text{total}}}. \quad \text{eqn S14}$$

We can express the diffusion coefficient D using Chapman–Enskog theory (variables defined in Table S1):

$$D_i \left(\frac{\text{m}^2}{\text{s}} \right) = \frac{\gamma \cdot T_{\text{BL}}^{\frac{3}{2}} \cdot \sqrt{1/M_i + 1/M_{\text{N}_2}}}{P_{\text{BL}} \cdot \sigma_i^2 \cdot \Omega_i}. \quad \text{eqn S15}$$

Note that the temperature (T_{BL}) and pressure (P_{BL}) in equation S15 are the temperatures and pressures relevant for diffusion across the boundary layer. T_{BL} is bounded by the chamber temperature (T_g) and the substrate temperature (T_s): $T_s < T_{\text{BL}} < T_g$, and P_{BL} is bounded by the deposition pressure and the stagnation pressure given by the Bernoulli eqn: $P < P_{\text{BL}} < P + \frac{1}{2} \rho \cdot v^2$.

Where v = flow velocity = $\frac{\dot{V}_{\text{total}}}{A_{\text{chamb}}} \cdot \frac{P_0}{P} \cdot \frac{T_g}{T_0}$ and ρ = density of chamber gas $\frac{P}{T_g} \cdot \frac{MM_{\text{N}_2}}{R}$.

For stagnation flow, the boundary layer thickness (δ) typically has a dependence on Re such as:²

$$\delta \cong \frac{C_3}{\sqrt{\text{Re}}} \quad \text{eqn S16}$$

Where Re = Reynolds number = $\frac{\rho v L}{\mu}$, L = relevant length scale = $2 \cdot r_{\text{chamb}}$, and μ = dynamic viscosity.

Thus,

$$\delta \cong \frac{C_3}{\sqrt{\rho v L / \mu}} = \frac{C_3 \sqrt{\mu}}{\sqrt{\frac{\dot{V}_{\text{total}}}{A_{\text{chamb}}} \cdot \frac{P_0}{T_0} \cdot \frac{MM_{\text{N}_2}}{R} \cdot 2 \cdot r_{\text{chamb}}}} \quad \text{eqn S17}$$

The viscosity of gasses at these pressures is relatively independent of pressure but depends strongly on temperature. The Sutherland formula states:

$$\mu = \mu_0 \frac{T_0 + \beta}{T + \beta} \left(\frac{T}{T_0} \right)^{3/2}. \quad \text{eqn S18}$$

Here μ_0 , T_0 , and β are constants tabulated for a specific gas. Rearranging and consolidating, we get

$$\mu = \mu_0 \cdot \frac{T_0 + \beta}{(T_0)^{3/2}} \cdot \frac{(T_g)^{3/2}}{T_g + \beta}. \quad \text{eqn S19}$$

Combining equations S17 – S19 and isolating the pertinent experimental variables, we get

$$\delta \cong C_{3,i} \sqrt{\frac{T_g^{3/2}}{\dot{V}_{\text{total}}(T_g + \beta)}} \sqrt{\mu_0 \cdot \frac{T_0 + \beta}{(T_0)^{3/2}} \cdot \frac{\pi r_{\text{chamb}} RT_0}{2 \cdot MM_{N_2} P_0}}. \quad \text{eqn S20}$$

Combining equations S13, S14, S15, and S20 and isolating relevant experimental parameters:

$$\begin{aligned} r_{\text{diff},i} \left(\frac{\text{mol}}{\text{s}} \right) &= \frac{\alpha_i}{C_{3,i}} \cdot \frac{T_{\text{BL}}^3}{P_{\text{BL}}} \cdot \frac{P_i}{T_i} \cdot \frac{\dot{V}_{\text{CG},i}}{\sqrt{\dot{V}_{\text{total}} \frac{T_g^{3/2}}{T_g + \beta}}}, \\ \alpha_i &= \frac{A_{\text{SH}} \gamma \sqrt{1/M_i + 1/M_{N_2}}}{\sigma_i z^2 \Omega_i} \cdot \frac{R}{\sqrt{\mu_0 \frac{T_0 + \beta}{(T_0)^{3/2}} \cdot \frac{\pi r_{\text{chamb}} RT_0}{2 \cdot MM_{N_2} P_0}}}. \end{aligned} \quad \text{eqns S21}$$

Plugging eqns S11 and S21 into eqn S3 will yield a full description of the flux of a species i onto the surface of the substrate; if the sticking coefficient is unity this will correspond to the deposition rate in mol/s. If this is the case, we can convert to $\text{\AA}/\text{s}$:

$$r_{\text{dep},i} \left(\frac{\text{\AA}}{\text{s}} \right) = r_i \left(\frac{\text{mol}}{\text{s}} \right) \cdot \frac{10^{10} M_i}{\rho_i A_{\text{chamb}}}. \quad \text{eqn S22}$$

Co-deposition Rate Derivation

For co-deposition, where two precursors A (*e.g.*, MABr) and B (*e.g.*, SnBr₂) are deposited simultaneously and react to form a perovskite on the substrate, the flux rates for each precursor can be converted to a deposition rate for the perovskite.

If the flux rates are equal, then the number of moles of perovskite reaching the surface of the film are the same as the flux of the precursor:

$$r_A \left(\frac{\text{mol}}{\text{s}} \right) = r_B \left(\frac{\text{mol}}{\text{s}} \right) = r_{\text{perovskite}} \left(\frac{\text{mol}}{\text{s}} \right). \quad \text{eqn S23}$$

If we assume a sticking coefficient of 1 and a 100% reaction rate, we can convert this to $\text{\AA}/\text{s}$

$$r_{\text{dep,perovskite}} \left(\frac{\text{\AA}}{\text{s}} \right) = r_{\text{perovskite}} \left(\frac{\text{mol}}{\text{s}} \right) \cdot \frac{10^{10} M_{\text{perovskite}}}{\rho_{\text{perovskite}} A_{\text{chamb}}}. \quad \text{eqn S24}$$

However, if the molar fluxes are not equal (*i.e.*, $r_A \neq r_B$), we can envision two limiting cases for the total film deposition rate:

1. Minimum Flux Limited

In this case, the excess precursor is rejected from the film, and the molar deposition rate of the perovskite is equivalent to the minimum molar flux of the two precursors:

$$r_{perovskite} \left(\frac{\text{mol}}{\text{s}} \right) = \min(r_A, r_B) \quad \text{eqn S25}$$

and

$$r_{\text{dep,perovskite}} \left(\frac{\text{\AA}}{\text{s}} \right) = \min(r_A, r_B) \cdot \frac{10^{10} M_{perovskite}}{\rho_{perovskite} A_{\text{chamb}}} \quad \text{eqn S26}$$

2. Total Flux

If the excess precursor is not rejected, the total deposition rate will be the sum of the perovskite deposition plus the deposition of the excess precursor phase:

$$r_{\text{dep,perovskite}} \left(\frac{\text{\AA}}{\text{s}} \right) = \min(r_A, r_B) \cdot \frac{10^{10} M_{perovskite}}{\rho_{perovskite} A_{\text{chamb}}} + |r_A - r_B| \cdot \frac{10^{10} M_{\max(A,B)}}{\rho_{\max(A,B)} A_{\text{chamb}}} \quad \text{eqn S27}$$

Simplifications for Depositions Reported Herein

There are two major simplifications that apply to the depositions reported herein:

1. Diffusion across boundary layer is not rate limiting $\rightarrow r_i \cong r_{\text{conv},i}$

For laminar, large Reynolds number (*Re*) flows ($500 \ll \text{Re} \ll 2000$), diffusion through the momentum boundary layer can be a rate limiting factor, and must be taken into account to accurately model deposition rates.² At the pressures and flow rates used in this study, however, $\text{Re} \ll 500$, and the momentum boundary layer does not have a significant impact on the overall deposition rate. In other words, $r_i \cong r_{\text{conv},i}$.

This relative unimportance of diffusive transport in this technique is quite convenient because it means that the radial nonuniformities in boundary layer thickness that exist for typical stagnation flow normal to a flat plate will not result in a significant variation of deposition rate across the substrate – reducing the need for a rotating substrate holder to achieve uniform film thickness.

Indeed, fitting our data including the diffusion term, we see $C_{3,i} \rightarrow 0$ and consequently $r_{\text{diff},i} \rightarrow \infty$ for all *i* reported herein. This is corroborated experimentally by the remarkable thickness uniformity we observe across our substrates.

2. Operating in “equilibrium regime” $\rightarrow P_i \cong P_{i,\text{eq}}$

Equation S9 implies two limiting regimes of deposition, as described in detail by Shtein et al.¹ In the “equilibrium” regime, source temperatures are high and carrier gas flow rates are low, and the vapor pressure in the ampoule is close to equilibrium. In this case, $\dot{V}_{\text{CG},i,\text{chamb}}/RT_i \rightarrow 0$ and $k_{\text{evap},i} \cong k_{\text{cond},i}$. In the “kinetic regime,” sublimed source material is carried out at rate high enough that equilibrium cannot be established, and the deposition rate depends on the surface area of source material in the ampoule via $k_{\text{evap},i}$ and $k_{\text{cond},i}$.

A schematic depiction of these two regimes can be seen in Fig. S1b. As the surface area of source material powder is difficult to control, it is desirable to avoid the kinetic regime all together, such that $P_i \cong P_{i,eq}$.

Using these two simplifying assumptions, we can re-write eqns S3 and S11 as eqn 1 in the main text:

$$r_i \left(\frac{\text{mol}}{\text{s}} \right) = C_{1,i} \cdot \frac{P_0 T_g}{RT_0} \cdot \frac{\dot{V}_{CG,i}}{P \cdot T_i} \cdot e^{-\frac{\Delta H_i^\ddagger}{R} \left(\frac{1}{T_i} - \frac{1}{C_{2,i}} \right)} \quad \text{eqn 1}$$

Supporting Figures

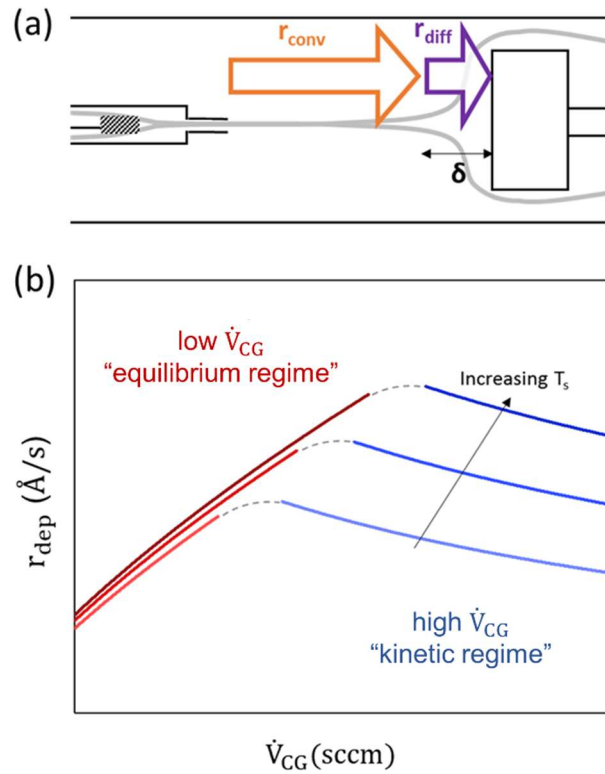
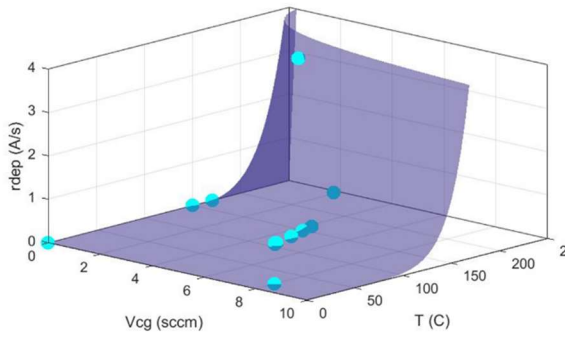
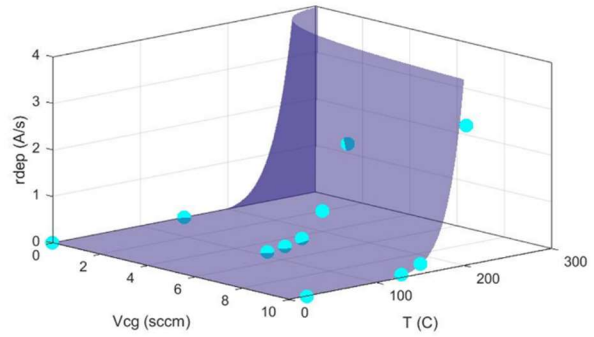


Fig. S1 (a) Regions of convective and diffusive transport of sublimed material vapor in CGAVD where the substrate is perpendicular to the gas flow. Convective transport carries the vapor from the source to the substrate boundary layer, diffusive transport occurs across the boundary layer (thickness δ). (b) Deposition rate as a function of carrier gas flow rate and source temperature for equilibrium and kinetic regimes. Operation in the equilibrium regime (*i.e.*, high source material temperature, low carrier gas flow rate) is desirable as the deposition rate is independent of source material surface area. In the kinetic regime, the source material vapor pressure is far below its equilibrium pressure, and as such depends on the surface area of the source material.

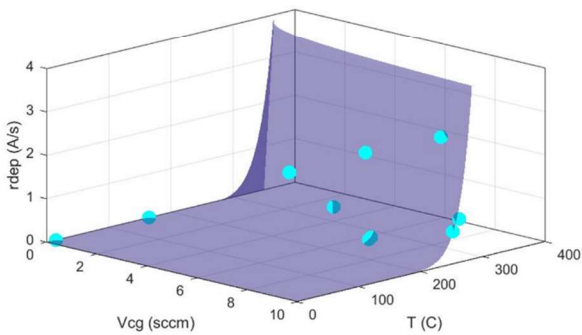
(a) **MABr**: $C_1=28$, $C_2=483$, $H=82.5$ [79, 85]



(b) **MAI**: $C_1=32$, $C_2=507$, $H=104$ [91, 115]



(c) **SnBr₂**: $C_1=29$, $C_2=565$, $H=140$ [126, 155]



(d) **SnI₂**: $C_1=29$, $C_2=602$, $H=180$ [175, 186]

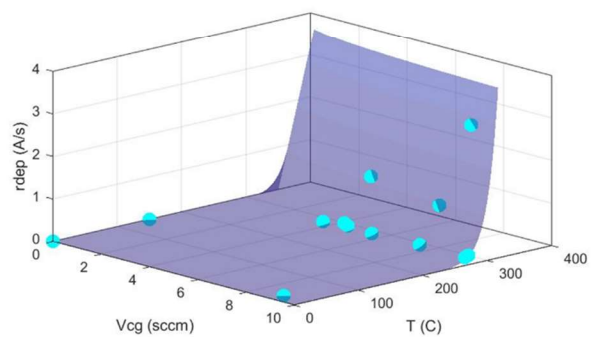


Fig. S2 Deposition rate data and fits of Equation 1 with corresponding fit parameters and 95% confidence intervals [in brackets] for (a) MABr; (b) MAI; (c) SnBr₂; and (d) SnI₂. Deposition rate was measured experimentally with the film thickness extracted using ellipsometry. Fits were performed with a non-linear least-square fit of Eqn. 1 in Matlab. Data shown here is for $P = 2.6$ Torr.

Table S2 Deposition parameters for films in Fig. 2.

(a,b) MASnBr₃

	MABr	SnBr ₂
$\dot{V}_{CG,i}$ (sccm)	3.5	5
T _i (°C)	147	246
\dot{V}_{DIL} (sccm)		192
T _g (°C)		280
T _s (°C)		20
P (Torr)		2.6
Film Thickness (nm)		450

(a,b) MASnBr_{1.5}I_{1.5}

	MABr	SnBr ₂	MAI	SnI ₂
	Deposition 1 (MASnBr ₃)		Deposition 2 (MASnI ₃)	
$\dot{V}_{CG,i}$ (sccm)	50	50	50	50
T _i (°C)	138	240	140	285
\dot{V}_{DIL} (sccm)		0		0
T _g (°C)		250		250
T _s (°C)		15		15
P (Torr)		1.3		1.3
Film Thickness (nm)		160		151

(a,b) MASnBr₂I

	MABr	SnBr ₂	MAI	SnI ₂
	Deposition 1 (MASnBr ₃)		Deposition 2 (MASnI ₃)	
$\dot{V}_{CG,i}$ (sccm)	5	17	5	12
T _i (°C)	136	246	150	287
\dot{V}_{DIL} (sccm)		177		175
T _g (°C)		280		280
T _s (°C)		15		15
P (Torr)		10		10
Film Thickness (nm)		91		49

(a,b) MASnI₃

	MAI	SnI ₂
$\dot{V}_{CG,i}$ (sccm)	5	12
T _i (°C)	149	287
\dot{V}_{DIL} (sccm)		183
T _g (°C)		280
T _s (°C)		15
P (Torr)		2.6
Film Thickness (nm)		410

(c) MASnBr₃

	MABr	SnBr ₂
$\dot{V}_{CG,i}$ (sccm)	4	5
T _i (°C)	139	221
\dot{V}_{DIL} (sccm)		90
T _g (°C)		280
T _s (°C)		45
P (Torr)		0.7
Film Thickness (nm)		125

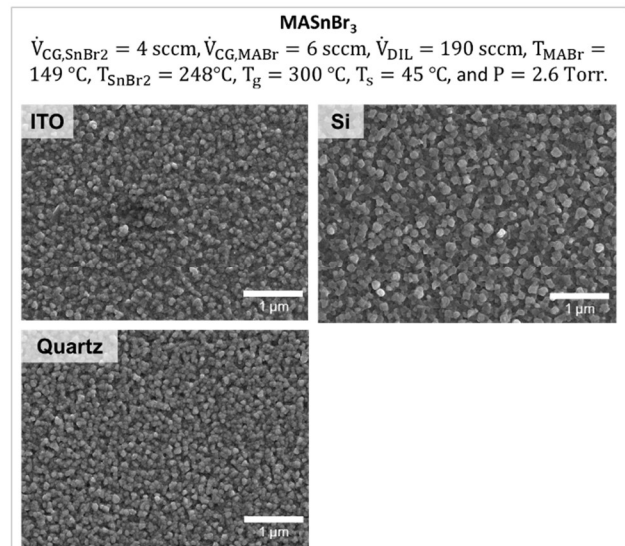
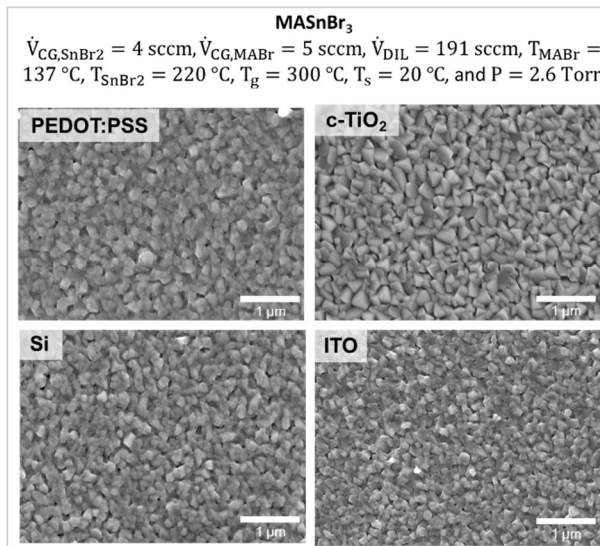
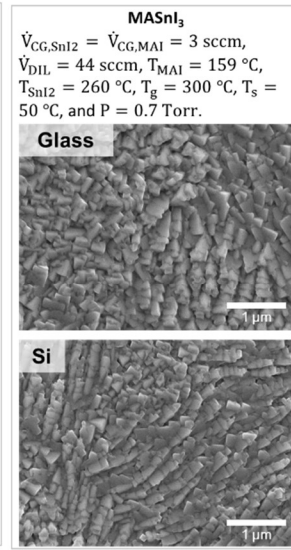
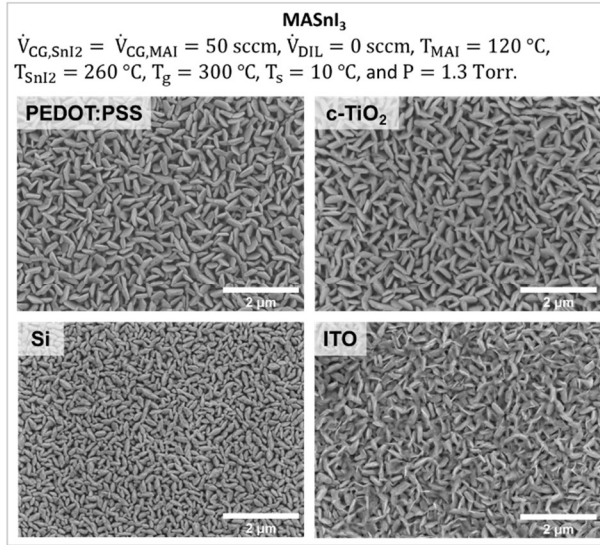


Fig. S3 MASnX₃ morphological consistency across various substrate types for stated deposition conditions. Not all morphologies pictured are ideal for device applications, however the morphology of these films appears to vary more as a function of deposition conditions than substrate type.

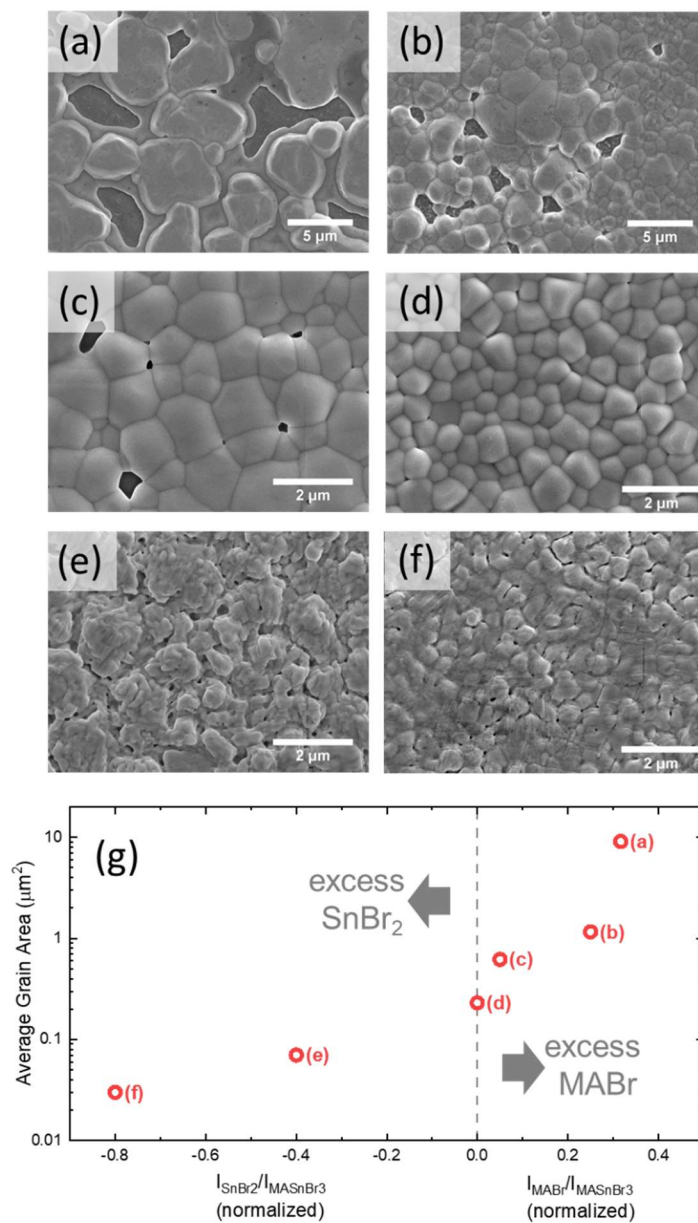


Fig. S4 (a)-(f) SEM micrographs and (g) corresponding grain sizes of films with varying amounts of excess MABr or SnBr₂. Excess MABr results in large grain areas of >1 μm², but films have significant pinholes/voids. Excess SnBr₂ results in morphologies have significant non-uniformities, have smaller grain sizes <0.1 μm², and less distinct grain boundaries. See Table S3 for deposition conditions, Fig. S6 for grain boundary images, and Fig. S5 for XRD patterns for films (a) – (f).

Table S3 Deposition parameters for films in Fig. S4.

	(a)		(b)		(c)		(d)		(e)		(f)	
	MABr	SnBr ₂										
$\dot{V}_{CG,i}$ (sccm)	4	3	4	3.5	4	3.3	3.3	5	3.3	5.4	3.3	5.4
T_i (°C)	151	249	154	250	151	249	147	246	148	247	148	252
\dot{V}_{DIL} (sccm)	193		192		193		192		191		191	
T_g (°C)	280		280		280		280		280		280	
T_s (°C)	15		15		15		15		15		15	
P (Torr)	2.6		2.6		2.6		2.6		2.6		2.6	

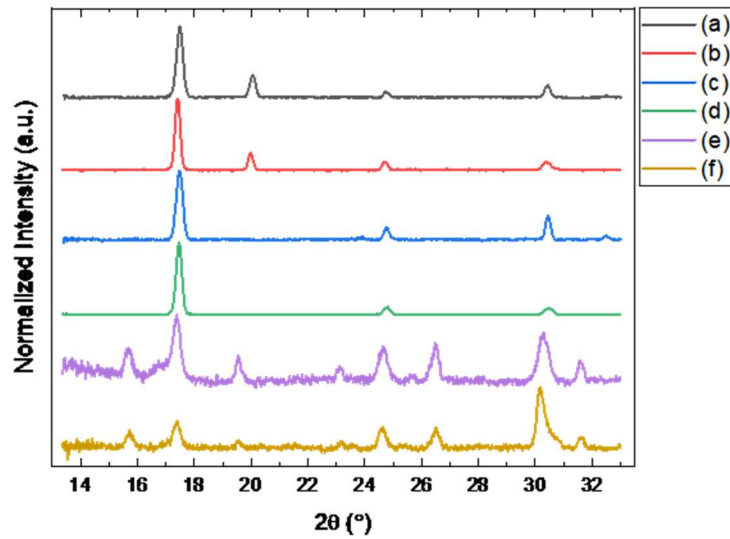


Fig. S5 X-ray diffraction patterns corresponding to films shown Fig. S4.

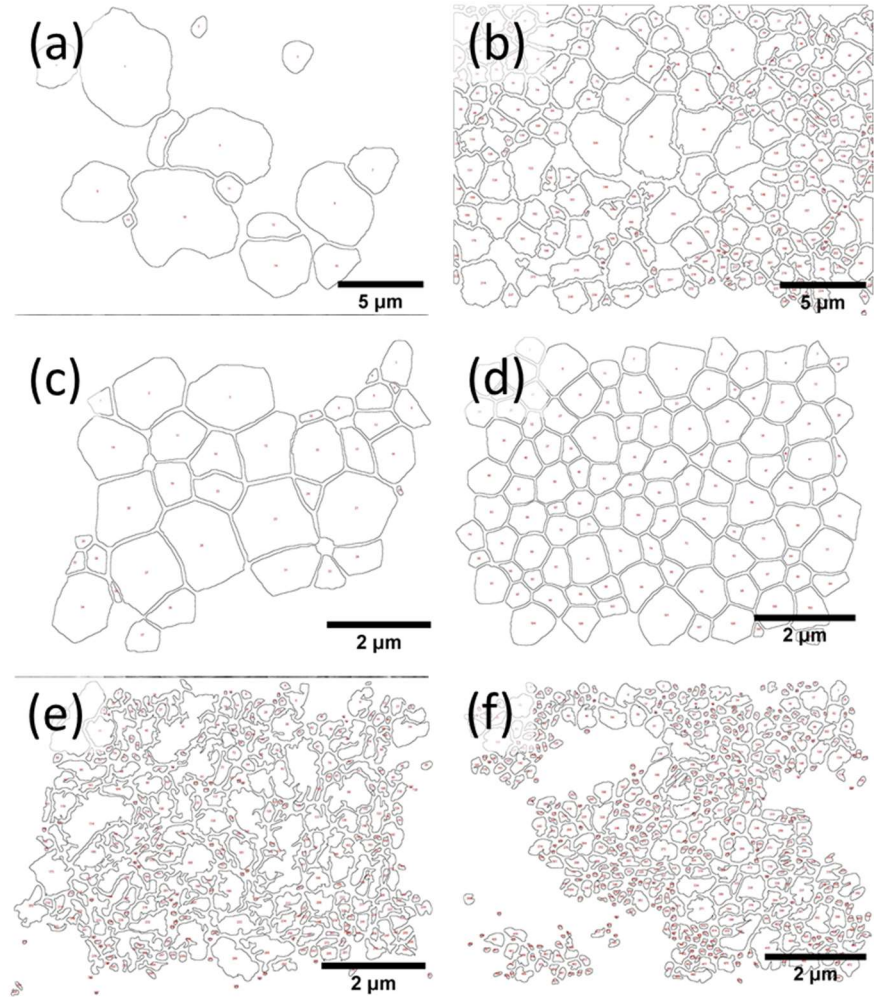


Fig. S6 Images used for grain size determination for SEM images in Fig. S4.

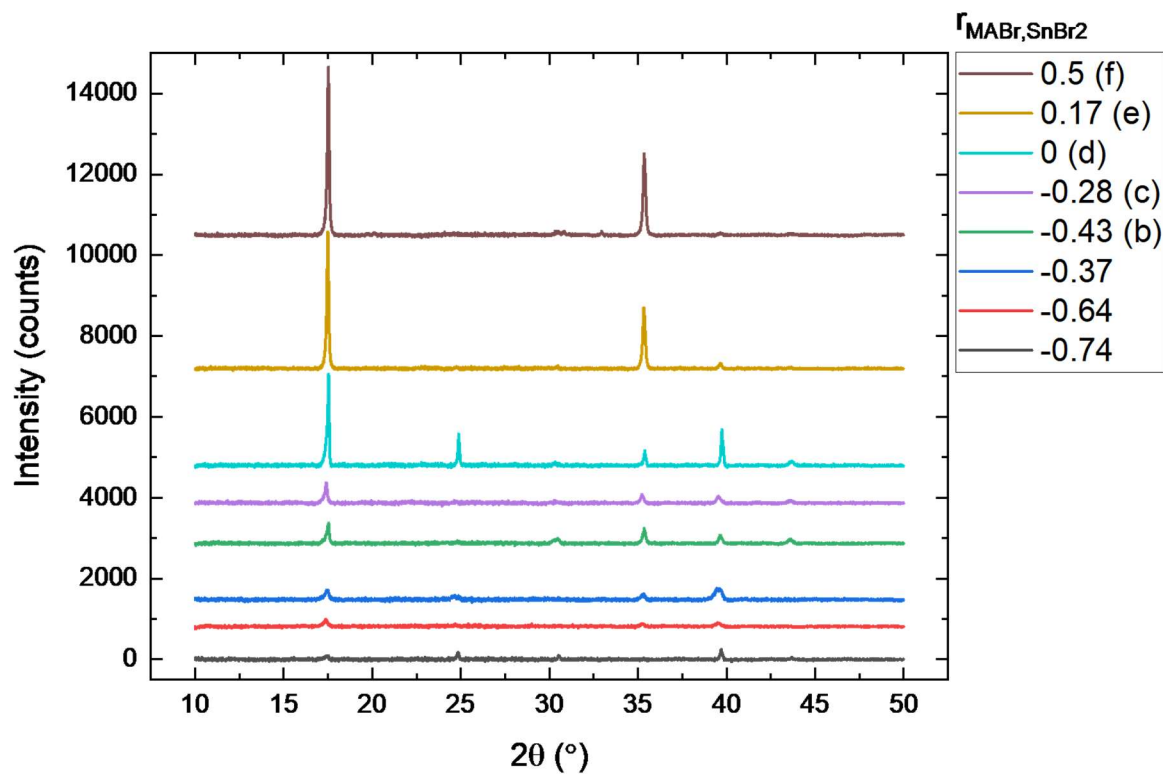


Fig. S7 X-ray diffraction patterns of MASnBr_3 films on quartz corresponding to XRD peak heights reported in Fig. 4a. Letters (b) – (f) correspond to the SEM images in Fig. 4.

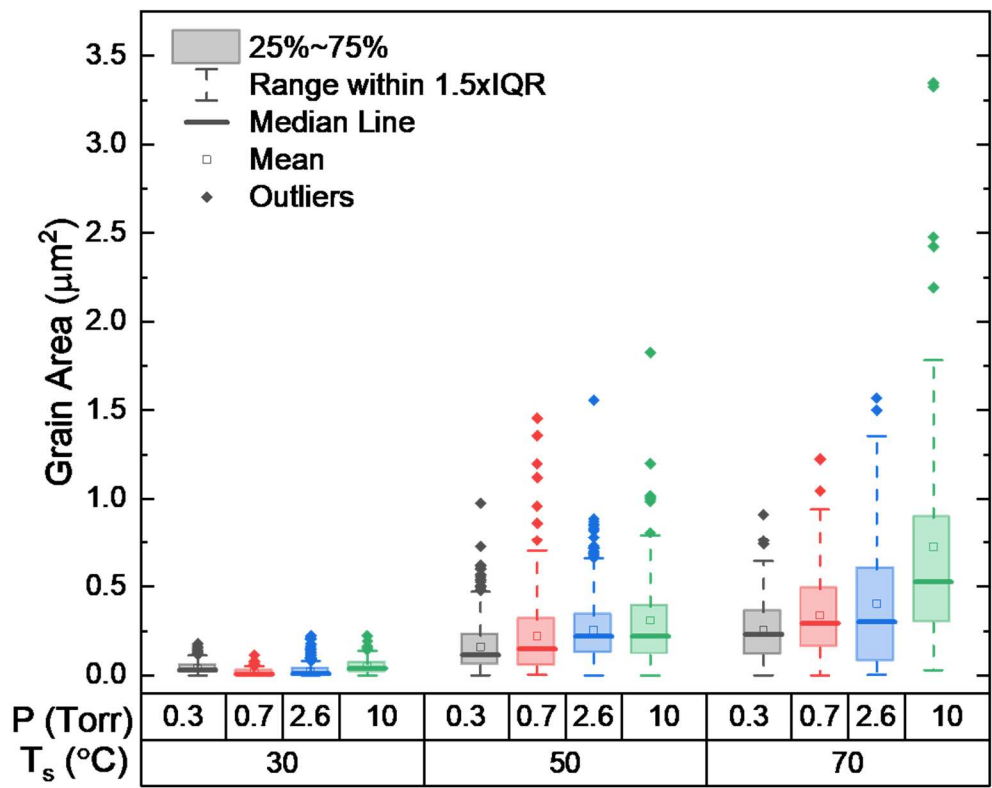


Fig. S8 Grain area distributions vs. P and T_s corresponding to MASnBr₃ films on quartz in Fig. 5 and Fig. S9. IQR corresponds to the interquartile range. Each distribution contains between 200 and 300 grains, taken from several SEM images from different areas on each substrate.

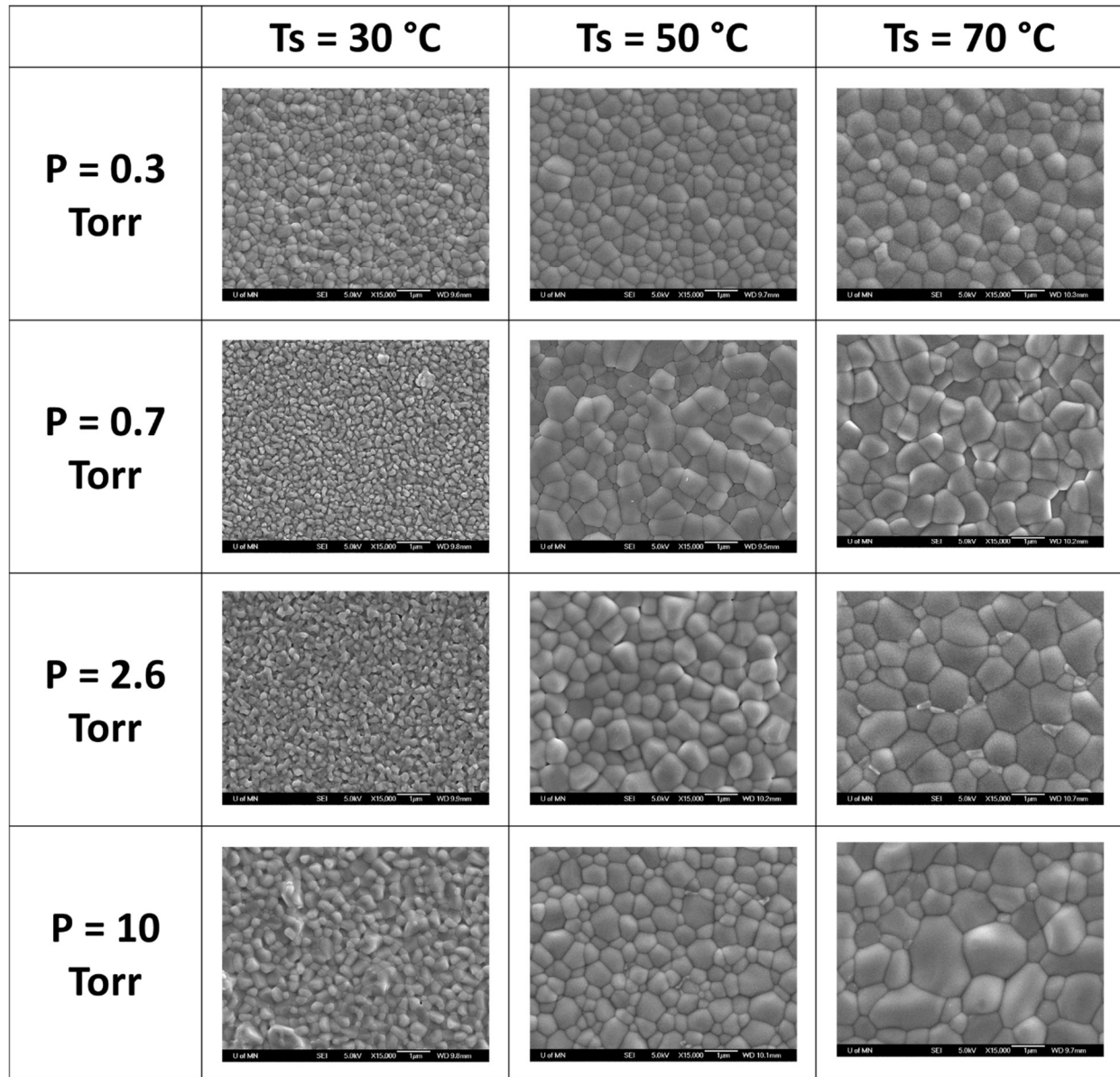


Fig. S9 SEM images corresponding to films in Fig. 5 and Fig. S8. All scale bars are 1 micron.

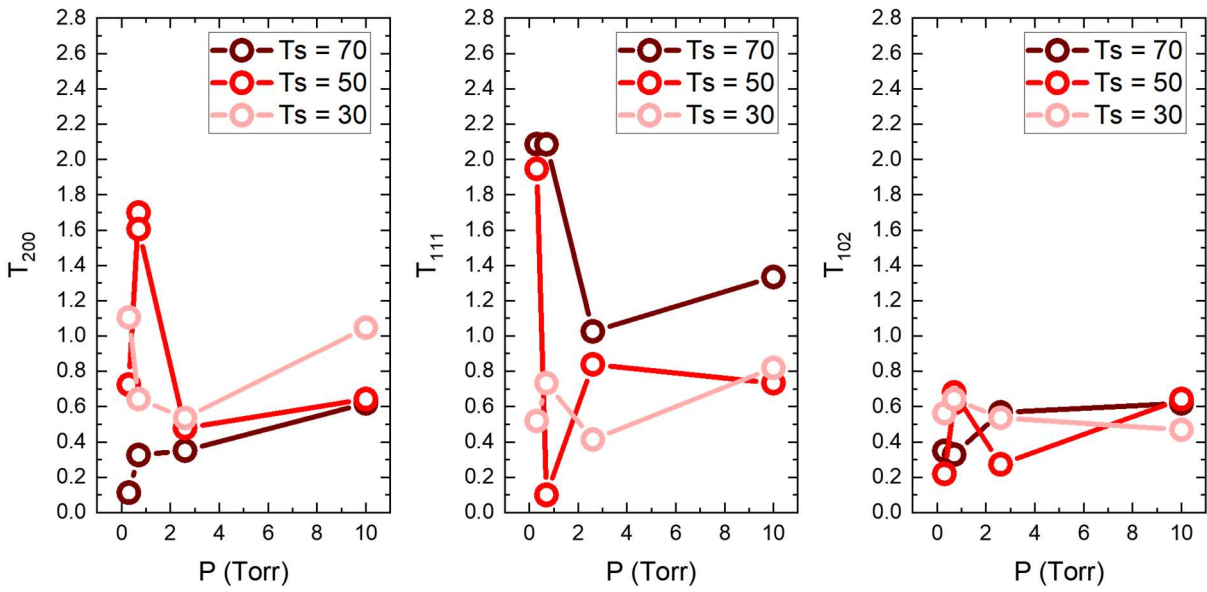


Fig. S10 Texture coefficient $TC_{h_i k_i l_i}$ as a function of P and T_s for additional peaks corresponding to Fig. 5. All other variables remained constant for these depositions: $\dot{V}_{CG, SnBr_2} = 4$ sccm, $\dot{V}_{CG, MABr} = 3$ sccm, $\dot{V}_{DIL} = 20$ sccm (for $P < 2.6$ Torr) or $\dot{V}_{DIL} = 200$ sccm (for $P \geq 2.6$ Torr), $T_{SnBr_2} = 233$ °C, $T_{MABr} = 142$ °C, and $T_g = 300$ °C.

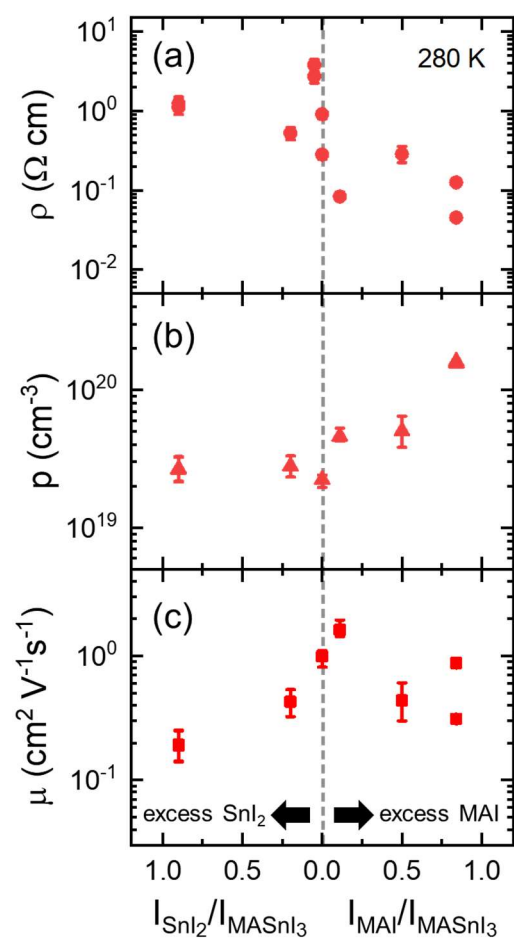


Fig. S11 (a) Resistivity (ρ), (b) hole concentration (p), and (c) Hall mobility (μ) of MASn_3 films as a function of stoichiometry. Error bars on p and μ include random uncertainty from the linear regression of the field dependence of the Hall resistance and uncertainty in film thickness. In nearly all cases, uncertainty from film thickness dominated. For these depositions, $\dot{V}_{\text{CG, SnI}_2} = 3$ sccm, $\dot{V}_{\text{CG, MAI}} = 3$ sccm, $\dot{V}_{\text{DIL}} = 44$ sccm, $P = 0.65$ Torr, $T_{\text{SnI}_2} = 270 - 275$ °C, $T_{\text{MAI}} = 154 - 161$ °C, and $T_g = 300$ °C. XRD patterns for these films are shown in Fig. S12, and representative Hall resistance vs magnetic field data is shown in Fig. S13.

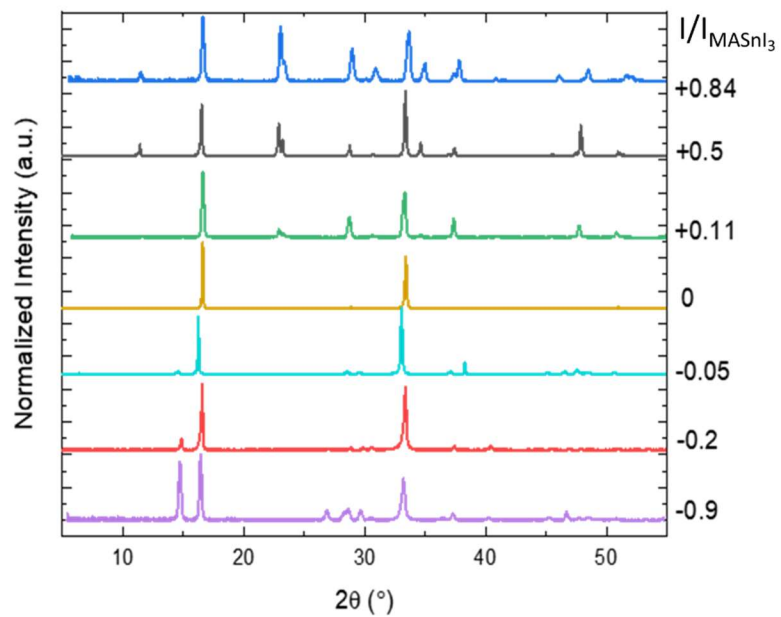


Fig. S12 X-ray diffraction patterns corresponding to films in Fig. S11. Normalized excess precursor ratios ($I_{\text{MAI}}/I_{\text{MASnI}_3}$ or $I_{\text{SnI}_2}/I_{\text{MASnI}_3}$) are listed to the right of the graph, with positive numbers indicating excess MAI and negative numbers indicating excess SnI_2 .

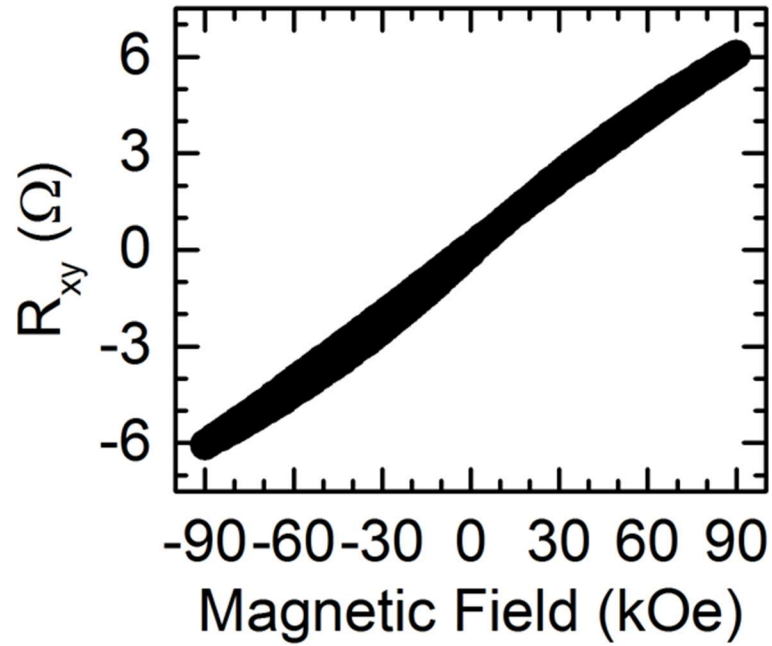


Fig. S13 The magnetic field dependence of the transverse (Hall) resistance (R_{xy}) for a stoichiometric MASnI_3 film (normalized excess precursor = 0 in Fig S11) at 280 K. The positive slope indicates p -type majority carriers, with the slope inversely proportional to hole concentration.

References

- 1 M. Shtein, H. F. Gossenberger, J. B. Benziger and S. R. Forrest, *J. Appl. Phys.*, 2001, **89**, 1470–1476.
- 2 D. S. Dandy and J. Yun, *J. Mater. Res.*, 1997, **12**, 1112–1121.